Supporting Information for "**Primary Photodynamics of the Green/Red-absorbing Photoswitching Regulator of Chromatic Adaptation E Domain from *Fremyella Diplosiphon*"**

Sean M. Gottlieb[1#], Peter W. Kim[1#], Yuu Hirose[3], Nathan C. Rockwell[2], Masahiko Ikeuchi[3], J. Clark Lagarias[2], Delmar S. Larsen[1]*

[1]Department of Chemistry
University of California, Davis
One Shields Ave, Davis, 95616

[2] Department of Molecular and Cell Biology
University of California, Davis
One Shields Ave, Davis, CA, 95616

[3]Department of Life Sciences (Biology),
University of Tokyo, 3-8-1 Komaba, Meguro-ku, Tokyo 153-8902, Japan

Target Analysis of Data

Two target models were constructed to fit broadband data from the forward reaction dynamics: a sequential-photoproduct' model (Figure S2) and a 'parallel-photoproduct' model (Figure S3). Both models are capable of describing the forward reaction dynamics for both 490-nm and 575-nm excitation datasets.

This 'sequential-photoproduct is shown in Figure S2A, with the resulting excitation-wavelength dependent SADS and concentration profiles presented in Figure S2C and S2E. This model fits both DEWI datasets well (Figure S2D and S2F, solid lines). We postulate that the multi-exponential decay of P_g* originates from multiple ground-state populations similar to those resolved in the reaction of the green-absorbing state of NpR6012g4 (*22*). While models with a single ground-state population could adequately fit the PP data, as does the sequential model in Figure 5, they cannot explain the wavelength-dependent fluorescence of RcaE (Figure S1). We therefore constructed a heterogeneous target model with several constraints:

1. The faster 2-ps and 10-ps decay phases of P_g* do not generate ^{15E}Lumi-G_1, consistent with the lack of spectral evolution in the normalized EADS1, EADS2 and EADS3 of the sequential global model (Figure 5). ^{15E}Lumi-G_1 is generated only from the slower 100-ps and 510-ps populations.
2. The SADS of the three excited-state intermediates (ESI) for each dataset are constrained to be identical, consistent with the nearly identical EADS1, EADS2, and EADS3 (Figure 5). However, the SADS of the 490-nm and 575-nm excitation data are not locked with each other.
3. Since ^{15E}Lumi-G_1 and ^{15E}Lumi-G_2 are ground-state species, their SADS must not contain excited-state ESA and SE signals (Figure S2). A postulated ^{15E}Lumi-G_1 → ^{15E}Lumi-G_2

transition exhibits a spectral narrowing, substantiated by the 1-ns and 2.5-ns spectra measured with significantly higher averaging (Figure 6 for 1-ns and 2.5-ns spectra, respectively). It is also possible to construct an alternative target model (Figure S3) in which ^{15E}Lumi-G_1 and ^{15E}Lumi-G_2 instead arise independently from different ground-state sub-populations. This model also fits the data, and PP spectroscopy alone cannot resolve these possibilities. We favor evolution of ^{15E}Lumi-G_1 into ^{15E}Lumi-G_2 by analogy to the reverse reaction of NpR6012g4 (*22*).

The species-associated difference spectra (SADS) derived from the target model are shown for both DEWI datasets in Figures S2C and S2E, with each P_g* SADS normalized at the red-most SE band of the ESI SADS (λ_{peak} = 630 nm). The SADS of ESI1, ESI2, and ESI3 are constrained to be identical. The ESI SADS for the 490-nm and 575-nm excitation data show clear differences below 560 nm, consistent with the raw data and with the preliminary sequential EADS analysis. The SADS of ^{15E}Lumi-G_1 exhibit broad absorption bands from 560 to 640 nm in both datasets, though the ground-state bleach bands are distinctly shifted from one another. Both datasets also exhibit a small positive region at approximately 680 nm which was not seen in characterization of the green-absorbing state of NpR6012g4 (*22*), but low signal-to-noise precluded its analysis.

490-nm excitation results in faster decay of the P_g* population and slightly greater Φ. Within the postulated inhomogeneous target model, the more productive (and faster decaying) ESI2 sub-population is preferentially populated by 490-nm excitation. In contrast, the slower ESI3 ($\tau_{apparent}$ = 510 ps) sub-population is preferentially populated by 575-nm excitation (Figure S2A; bold black boxes and Table 1). We model this differential occupation of excited-state sub-populations as arising from the ground-state heterogeneity of RcaE (Figure S2A, excitation

occupancy % in bolded GS box), which was estimated from a the amplitudes of a parallel (three-exponential) analysis of the ESA band (separate from the other bands).

The partial decay of ^{15E}Lumi-G_2 at longer delay times (>1 ns) to the $^{15Z}P_g$ ground state is resolvable by the decay of both the GSB and ^{15E}Lumi-G_2 absorption bands (Figures 4B and D for GSB and ^{15E}Lumi-G_2, respectively). Moreover, the ^{15E}Lumi-G_2 population after 575-nm excitation exhibits faster decay kinetics (3.5 ns) than after 490-nm excitation (10 ns), which is consistent with the individual spectra measured with greater averaging (Figure 5). The source for this decay is not yet clear; it is possible that it reflects ongoing evolution into a subsequent *15E* state that cannot be distinguished from $^{15Z}P_g$ on this timescale.

The alternative 'parallel-photoproduct' tagart model (Figure S3) follows the same assumptions outline above with a fit to the date that is comparable to the ‘sequential-photoproduct’ model. Neither target models decompose the SADS into excitation-wavelength dependent sub-populations indicated by the DEWI data.

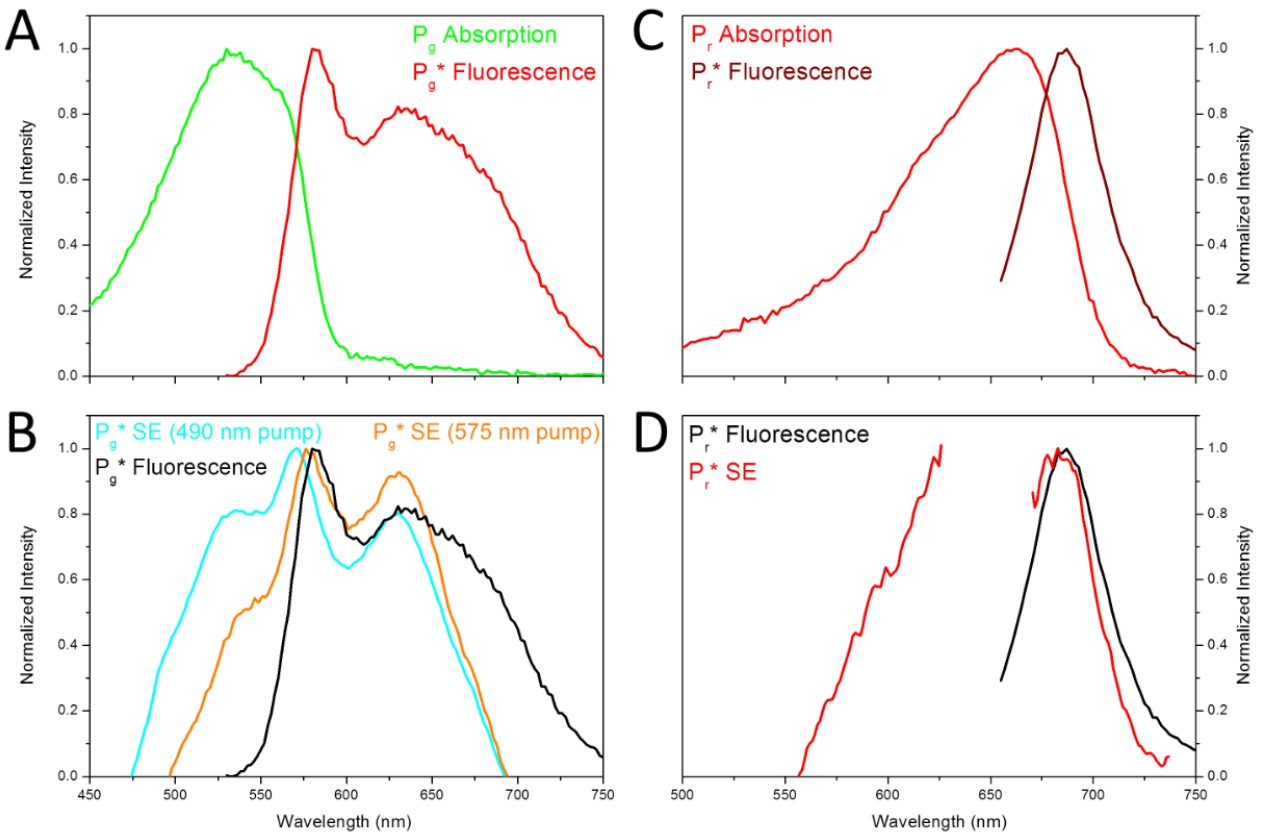

Figure S1: Static fluorescence of RcaE. (A) The fluorescence emission spectrum of RcaE (red) in the $^{15Z}P_g$ photostate is shown after excitation at 515 nm. The normalized absorption spectrum (green) is shown for comparison. (B) The fluorescence emission spectrum from (A) (black) is compared to inverted SE bands obtained upon application of pump pulses at 490 nm (cyan) or 575 nm (orange). (C) The fluorescence emission spectrum of RcaE (brick red) in the $^{15E}P_r$ photostate is shown. The normalized absorption spectrum (red) is shown for comparison. (D) The $^{15E}P_r$ emission spectrum from (C) (brick red) is compared to the inverted SE band obtained in PP spectroscopy.

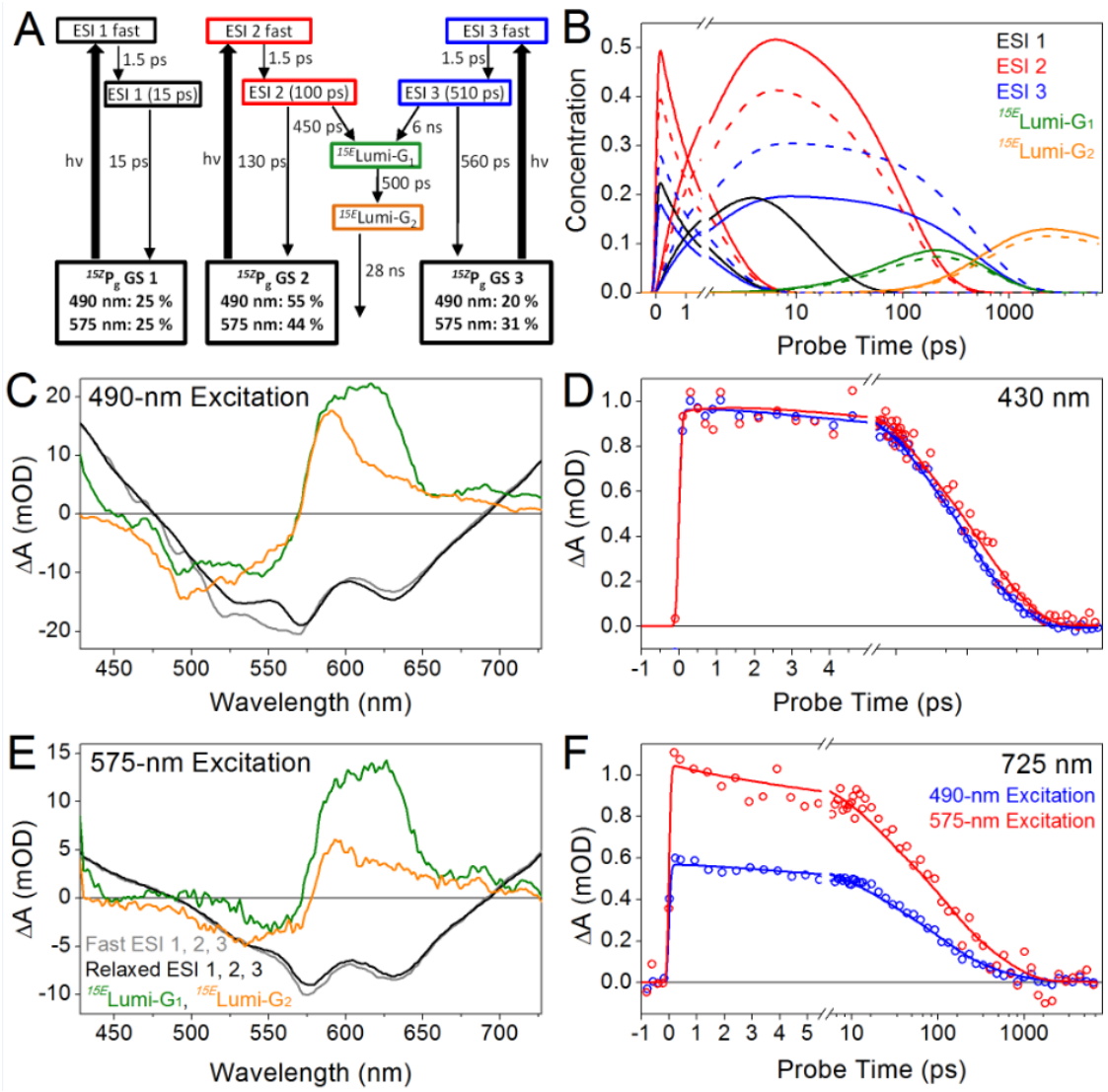

Figure S2: 'Sequential-Photoproduct' Target model of the forward reaction ($^{15Z}P_g$ excitation) consists of three ground-state populations (GS 1, 2 and 3) with excitation-dependent occupancy levels (%) as indicated. The lifetime of each state is identical for 490-nm and 575-nm excitation data, except for the ^{15E}Lumi-G_2 (green box) dynamics to the $^{15Z}P_g$ ground-state and/or subsequent photoproduct species. Each (ESI) has a 1.5-ps fast vibrational relaxation dynamic and subsequent slower dynamics either to the ground-state or to the primary photoproduct, ^{15E}Lumi-G_1.

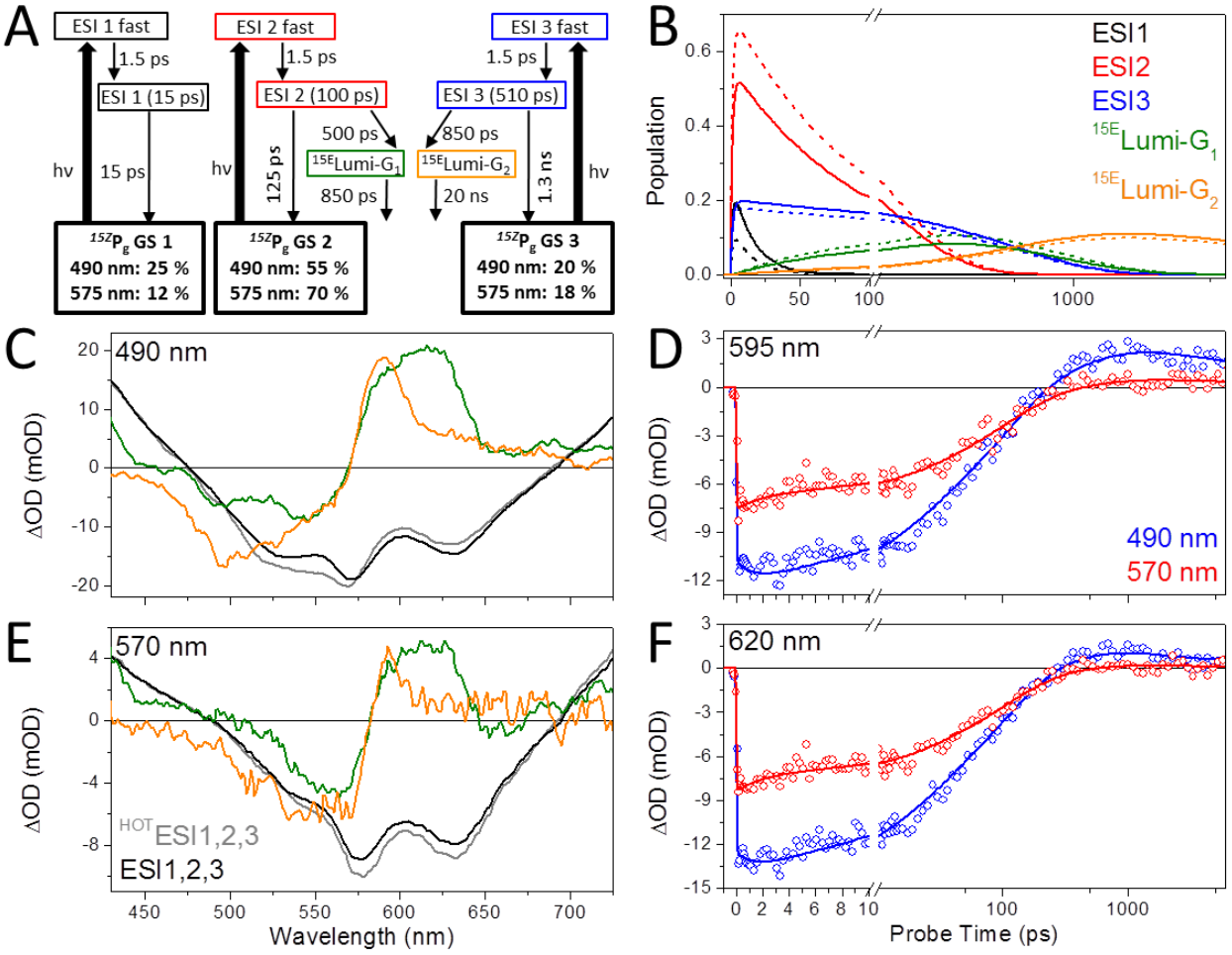

Figure S3: 'Parallel-Photoproduct' Target model of the forward reaction ($^{15Z}P_g$ excitation) (A) An alternate target model, in which Lumi-G_1 and Lumi-G_2 evolve in parallel from different excited-state sub-populations. (C) and (E) SADS for the alternate model are shown for the indicated excitation wavelengths. (B) Evolution of populations from the alternate target model in time. (D) and (F) Kinetic traces at the indicated wavelengths are shown for excitation at 490 nm (blue) and 575 nm (red).

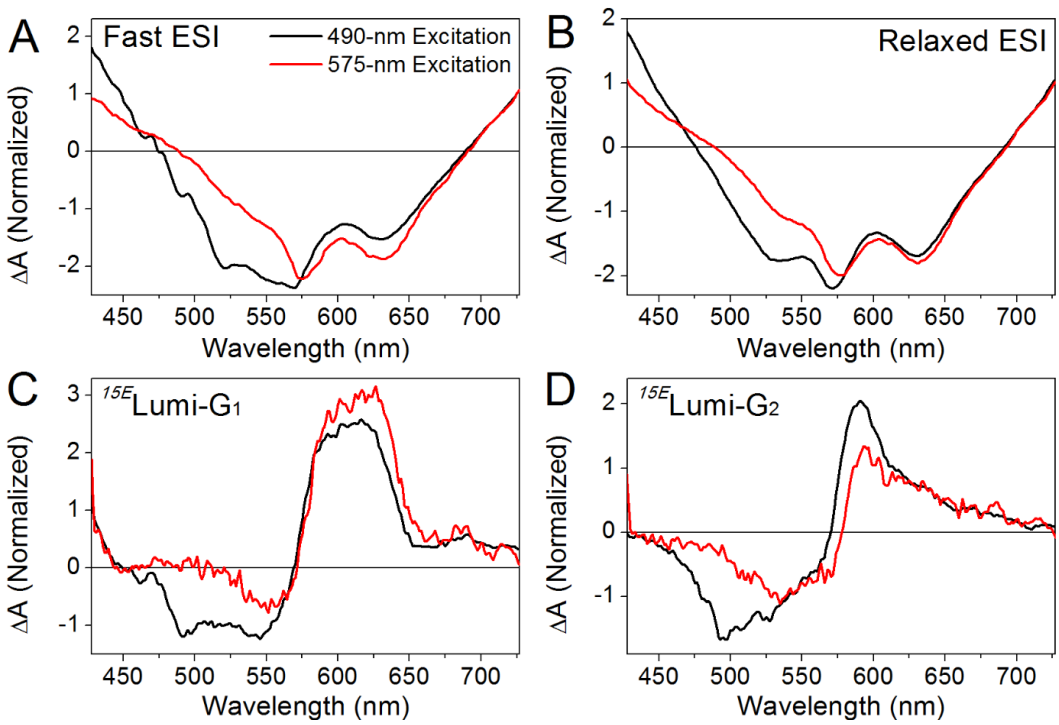

Figure S4: Comparison of DEWI SADS in Figure S2 between the 490-nm (solid black curves) and 575-nm (solid red curves) excitation datasets. (A,B) ESI, (C) ^{15E}Lumi-G_1 (D) and ^{15E}Lumi-G_2. Spectra were normalized to the ESA band near 720 nm for the ESI spectra.

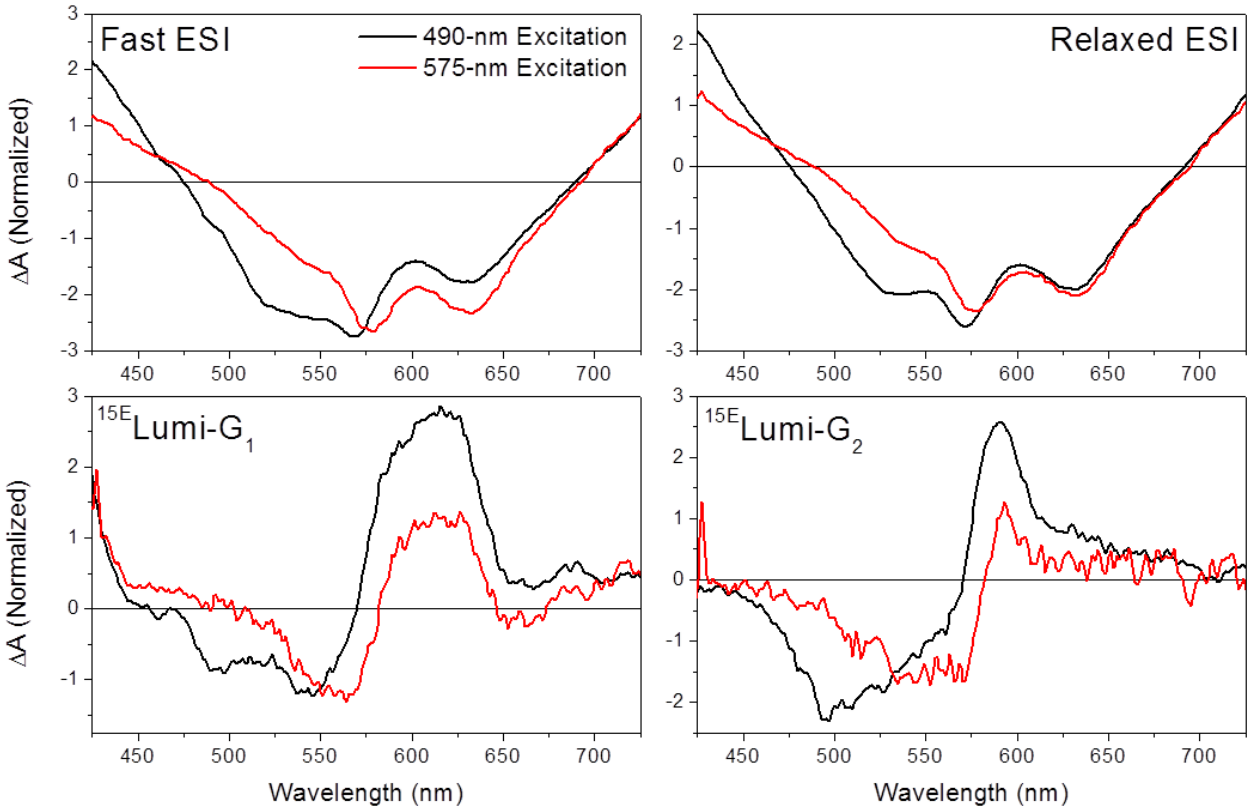

Figure S5: Comparison of DEWI SADS in Figure S3 between the 490-nm (solid black curves) and 575-nm (solid red curves) excitation datasets. ESI, ^{15E}Lumi-G_1 and ^{15E}Lumi-G_2. Spectra were normalized to the ESA band near 720 nm for the ESI spectra.

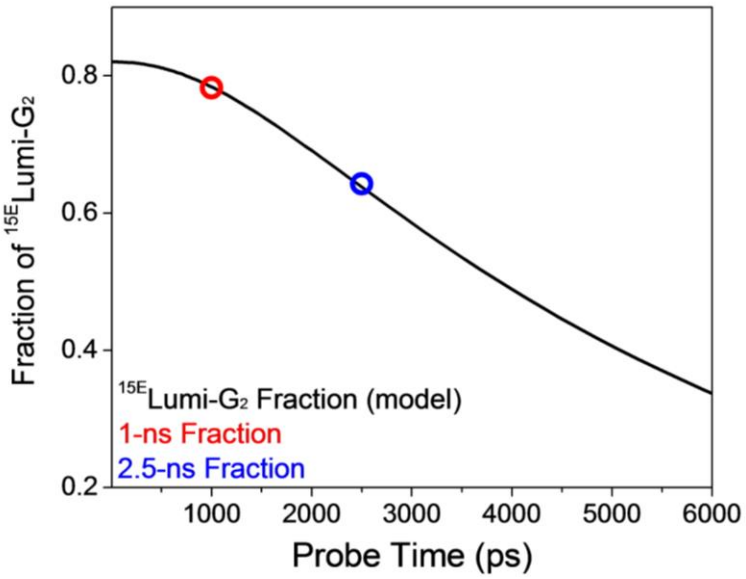

Figure S6: The ratio of excitation-dependent Lumi-G_2 populations, Lumi-G2 $_{575\text{-nm}/}$ Lumi-G2 $_{490\text{-nm}}$ (black line), was calculated based on the concentration profile (Fig. 9C) of the target model (Fig. 8). Red and blue circles indicate the averaged (from 580 to 610 nm, the peak region of the Lumi-G_2 spectrum) fraction of the normalized transient spectra at 1 ns and 2.5 ns (Fig. S3), respectively, showing excellent agreement with the kinetic model.

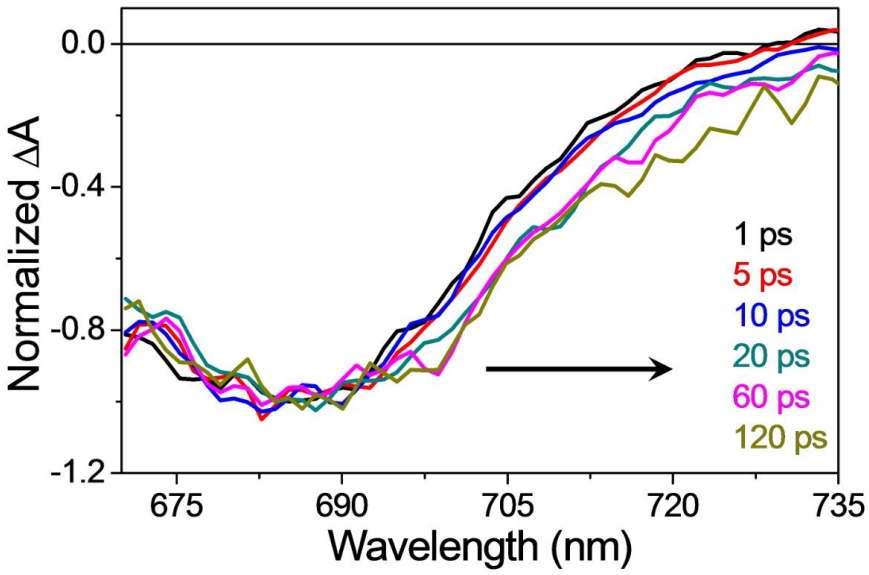

Figure S7: Normalized SE at select probe delay times. All spectra are scaled at the SE region near 690 nm to show broadening of that band over time. Arrow in the figure indicates the direction of spectral evolution at longer probe delay times.

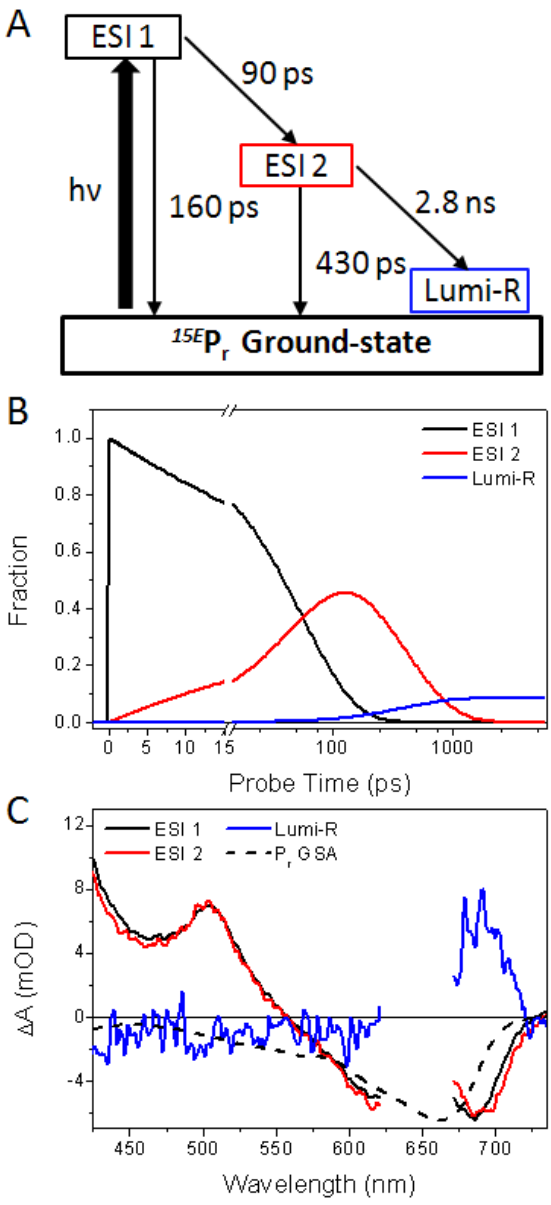

Figure S8: Target analysis of the reverse P_r excitation with a homogeneous three-component branched decaying model (A). Effective time constants of each population extracted from sequential analysis are conserved. (B) Population profile associated with the sequential model, tracking the flow of population through the excited-state intermediates, showing photoproduct **Φ** at approximately 10%. (C) Species-associated-difference spectra (SADS) estimated with proposed model. The spectral similarity between ESI1 and ESI2 suggests little structural deformation between these populations.

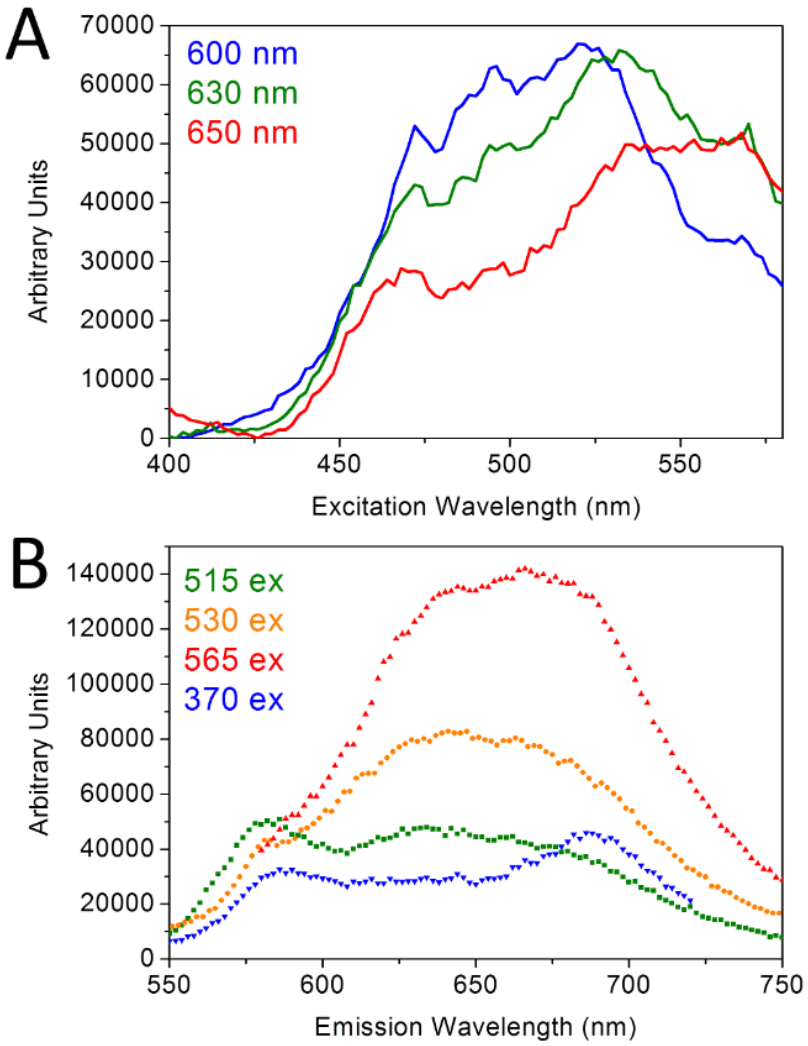

Figure S9: (A) Fluorescence excitation spectra of P_g. The emission is strongly dependent on the excitation wavelength. (B) Emission spectra collected after excitation at specific wavelengths.